
MemoryOut: Learning Principal Features via Multimodal Sparse Filtering Network for Semi-supervised Video Anomaly Detection

**Junlong Li ^{*1}, Lingwei Dang ^{*1}, Yukun Su ², Yun Hao ¹,
Qingxin Xiao ^{1,3}, Yongwei Nie ⁴, Qingyao Wu^{†1,3}**

¹School of Software Engineering, South China University of Technology

²Wechat AI, Tencent ³Institute for Super Robotics (Huangpu)

⁴School of Computer Science and Engineering, South China University of Technology

Abstract

Video Anomaly Detection (VAD) methods based on reconstruction or prediction face two critical challenges: (1) strong generalization capability often results in accurate reconstruction or prediction of abnormal events, making it difficult to distinguish normal from abnormal patterns; (2) reliance only on low-level appearance and motion cues limits their ability to identify high-level semantic in abnormal events from complex scenes. To address these limitations, we propose a novel VAD framework with two key innovations. First, to suppress excessive generalization, we introduce the Sparse Feature Filtering Module (SFFM) that employs bottleneck filters to dynamically and adaptively remove abnormal information from features. Unlike traditional memory modules, it does not need to memorize the normal prototypes across the training dataset. Further, we design the Mixture of Experts (MoE) architecture for SFFM. Each expert is responsible for extracting specialized principal features during running time, and different experts are selectively activated to ensure the diversity of the learned principal features. Second, to overcome the neglect of semantics in existing methods, we integrate a Vision-Language Model (VLM) to generate textual descriptions for video clips, enabling comprehensive joint modeling of semantic, appearance, and motion cues. Additionally, we enforce modality consistency through semantic similarity constraints and motion frame-difference contrastive loss. Extensive experiments on multiple public datasets validate the effectiveness of our multimodal joint modeling framework and sparse feature filtering paradigm. Project page at https://qzfm.github.io/sfn_vad_project_page/.

1 Introduction

Video Anomaly Detection (VAD) aims to automatically identify events that deviate from normal behavior patterns [40, 24]. Due to the lack of adequate and representative abnormal samples, current mainstream methods learn normal patterns from a large number of normal videos (Figure 1 (c)) and detect anomalies through reconstruction [10, 34, 11, 46] or prediction [3, 24, 25, 51, 36, 52] errors during inference.

Nevertheless, reconstruction/prediction approaches face two primary challenges. The first lies in the strong generalization ability of deep neural networks: abnormal events can also be well reconstructed

^{*}Equal contributions. Email: qlzjftm@gmail.com, levondang@163.com.

[†]Email: qyw@scut.edu.cn.

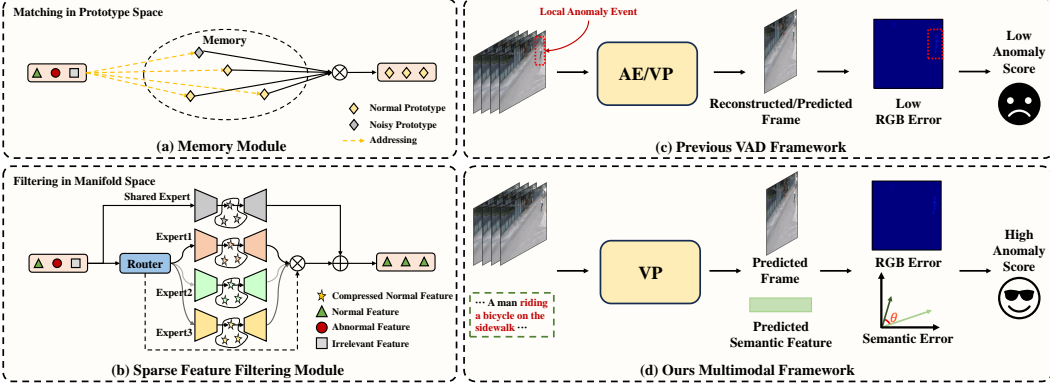


Figure 1: Comparison between previous and our proposed framework. (a) Existing memory modules filter anomalous information through inflexible prototype matching. (b) Our proposed sparse feature filtering paradigm achieves better VAD performance compared to memory-based methods. (c) Existing methods measure anomaly scores through reconstruction or prediction errors, which may produce smaller errors when dealing with small objects. (d) Our proposed novel multimodal framework introduces a semantic branch that can capture subtle local anomalies through semantic errors.

or predicted, making it hard to distinguish abnormal from normal events. To address this, several works [10, 51, 25, 21, 52] introduce memory modules (Figure 1 (a)) that store a set of prototypes representing the distribution of normal events. At test time, normal events match these prototypes and are reconstructed or predicted accurately, while anomalies that are not represented in the memory slots increase reconstruction or prediction errors. Nevertheless, memory-based methods lack flexibility and adaptability because of the fixed number of prototypes and are applied uniformly to every test sample, ignoring the difference and the diversity of complex scenes. If the memory prototypes do not encompass the full range of normal patterns, the model’s performance will suffer. An excessive number of prototypes will also lead to overly strong generalization and difficulties in optimization.

To overcome the above problem, in this paper, we propose the Sparse Feature Filtering Module (SFFM) (Figure 1 (b)) as an alternative to the memory modules. Inspired by bottleneck blocks [13, 15], which balance representational capacity and efficiency by extracting key information through bottleneck representations. These bottlenecks without skip connections will force the model to learn principal features, which are expected to capture only the key normal low-dimensional manifold, as they are trained solely on normal data. While abnormal information lies outside the learned feature space. Moreover, this bottleneck-based feature filtering paradigm, free from a rigid prototype matching process, offers greater flexibility and adaptability, allowing different principal features to be extracted for different events.

However, we observe that a single bottleneck is insufficient to model the diverse characteristics of normal patterns. Inspired by the Mixture of Experts (MoE) [6, 35, 20] architecture, we design multiple bottleneck filters and employ a router to automatically and selectively activate the most appropriate filtering experts and then aggregate. Each filtering expert is responsible for extracting specialized principal features, while a shared expert is used to extract common features, which enhances the feature filtering process with improved diversity and capacity. This design can achieve better performance than the memory module.

The second limitation of existing methods is that they only employ low-level appearance and motion as cues, which cannot capture subtle abnormal behaviors from RGB errors. If we reexamine anomalies at the semantic level, they can be regarded as a sudden change in the semantic logic of the context in a specific environment (e.g. a car appearing on the sidewalk), and we find that within several consecutive frames of time, normal events usually maintain semantic consistency, while the semantics of abnormal events are unpredictable. This inspires us that we can enhance the perception of high-level abstraction of abnormal events through semantics. Based on this insight, we propose a novel multimodal framework that introduce text descriptions of the input clips to joint model the three modal information of appearance, motion, and semantics simultaneously, and then jointly decode and predict future frames and semantic features simultaneously (Figure 1 (d)).

Finally, we have additionally introduced a novel multimodal consistency enhancement mechanism to support our framework. Through frame prediction loss, text semantic similarity loss, and motion frame-difference contrast loss, the consistency among visual prediction, semantics, and motion is guaranteed. Meanwhile, the anomaly score is measured based on the prediction errors of the visual and semantic modalities, achieving a more powerful semi-supervised anomaly detection capability.

Our contributions are summarized as follows:

- We propose a novel abnormal information filtering paradigm that combines bottleneck filters with MoE architecture to replace the memory module, thereby solving the problem of excessive generalization in complex scenarios in a more effective way.
- We implement a multimodal joint modeling framework that simultaneously models appearance, motion, and semantic information, comprehensively leveraging cross-modal cues to enhance sensitivity to a wide range of anomaly types.
- We introduce a multimodal consistency constraint mechanism to ensure the consistency among different modalities, enabling the simultaneous use of prediction and semantic errors for robust anomaly scoring.

2 Related Work

Video Anomaly Detection. Due to the difficulty of collecting abnormal data, existing approaches can be broadly classified into two paradigms: reconstruction [10, 34, 11, 46] and prediction [3, 24, 25, 51, 36, 52]. These methods can be further categorized as frame-centric methods [24, 10, 31, 46, 45, 16, 34, 21] or object-centric methods [47, 9, 25, 2, 36, 3]. The latter extracts foreground objects as processing units instead of entire frames through object detection or tracking techniques, which generally leads to better performance but incurs significant computational overhead. With the addition of semantic modality, our multimodal framework can outperform object-centric methods, relying solely on frame-centric inputs.

Memory networks. To prevent overgeneralization to abnormal data, some works [10, 51, 25, 21, 52, 31, 28] have introduced memory modules to store normal patterns in the training data. However, the fixed number of prototypes limits the diversity of features and ignores the differences in different scenarios. In addition, the effectiveness of memory modules relies on carefully configured settings, as improper settings may lead to excessive information filtering or unwanted generalization and training difficulties. Our bottleneck filter can achieve more flexible and adaptive feature filtering.

Mixture of Experts. Mixture of Experts (MoE) architecture [17, 7] has been widely explored to improve the computational efficiency of large language models [20, 35, 6, 22, 27]. Inspired by MoE and unlike typical efforts focused on reducing computation, we leverage MoE to amplify the representational capacity of the feature-filtering mechanism, with each expert specializing in extracting and compressing specific knowledge for finer-grained filtering.

Vision-Language Models. Recent advances in vision-language models (VLMs)[33, 18, 38, 14, 23] have enabled language models to understand visual content, and some video models[49, 30, 39, 5, 1] show promise in video understanding. Existing VLM-based methods [29, 50, 37] struggle with frame-level semi-supervised VAD. To capture abnormal behaviors more comprehensively, we propose a multimodal joint framework that leverages VLM to extract abnormal cues from appearance, motion, and semantics.

3 Method

The overall framework we propose, termed SFN-VAD, is illustrated in Figure 2. First, Tri-Modal Fusion Encoder (TMFE) (Section 3.2) encodes frames, frame differences, and captions to joint model appearance, motion, and semantic information. The processed features are then passed to the Multimodal Joint Attention Decoder (MJAD) (Section 3.4) for mutual assistance modeling. Each decoding layer incorporates an Sparse Feature Filtering Module (SFFM) (Section 3.3) to filter features, ensuring that only principal normal features are retained to accomplish the prediction tasks.

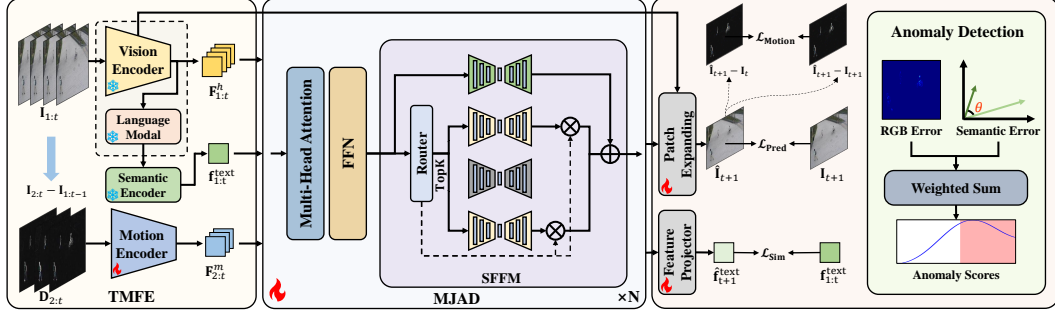


Figure 2: Overview of SFN-VAD. Firstly, TMFE extracts descriptions from the input clips and encodes and fuses semantic, appearance, and motion features. Secondly, MJAD performs joint decoding of the fused features to predict the next frame and semantic features. SFFM filters abnormal information to increase prediction error when anomalies occur. Finally, anomaly scores are calculated based on frame prediction errors and semantic errors.

Finally, we introduce the Inter-modality Consistency Constraint Mechanism to ensure the multimodal alignment (Section 3.5). In subsequent sections, we will first elaborate on the problem formulation (Section 3.1), then provide detailed explanations of these three modules, and finally show how to implement anomaly detection (Section 3.6).

3.1 Problem Definition

For a given video, our goal is to calculate the anomaly confidence for each frame. Following [24], we employ a prediction-based method where a video prediction model is trained on normal data. Mathematically, given consecutive video frames $\{\mathbf{I}_1, \mathbf{I}_2, \dots, \mathbf{I}_t\}$, the model predicts the next frame \mathbf{I}_{t+1} and its corresponding text semantic feature $\mathbf{f}_{t+1}^{\text{text}}$. During testing, both frame error and semantic error are used as the anomaly score.

3.2 Multimodal Feature Extraction

Vision Appearance Encoding Branch. Some works [4, 42, 41, 48, 32, 44] have attempted to apply VLM to weakly-supervised VAD, however, no existing research has yet explored their application in semi-supervised VAD tasks. Existing methods focus on appearance and motion, ignoring the semantic manifestation of anomalies. For joint modeling, we employ a VLM [5] to extract video descriptions of input video clips and visual embedding. Specifically, we first utilize the vision encoder Φ_v from the pre-trained VLM to extract visual embeddings for continuous video frames $\{\mathbf{I}_1, \mathbf{I}_2, \dots, \mathbf{I}_t\}$. This process can be mathematically expressed as:

$$\mathbf{F}_i^h = \Phi_v(\mathbf{I}_i), \text{ where } i = 1, 2, \dots, t. \quad (1)$$

Text Semantic Encoding Branch. With the extracted visual features, a language model [43] generates the video description $\mathbf{C}_{1:t}$ for the input video clip. To further obtain the semantic feature, we employ a pre-trained text encoder Φ_t [8] to extract semantic embeddings $\mathbf{f}_{1:t}^{\text{text}}$. These embeddings represent the semantic information of the entire video clip. Mathematically, this can be expressed as follows:

$$\mathbf{C}_{1:t} = \text{VLM}(\{\mathbf{I}_1, \mathbf{I}_2, \dots, \mathbf{I}_t\}, \mathbf{P}), \quad (2)$$

$$\mathbf{f}_{1:t}^{\text{text}} = \Phi_t(\mathbf{C}_{1:t}), \quad (3)$$

where $i = 1, 2, \dots, t$ and \mathbf{P} is a fixed textual prompt that provides instructions to the VLM.

Motion Dynamic Encoding Branch. Previous work [24, 25, 52, 34, 21] has demonstrated that motion information plays a crucial role in the VAD task. Unlike some methods [24, 25] that introduce optical flow as motion information, we use frame differences between adjacent frames to achieve faster processing speeds without the need for additional offline preprocessing. We train a ViT-based motion encoder Φ_m to encode motion information. The mathematical representation is as follows:

$$\mathbf{F}_i^m = \Phi_m(\mathbf{D}_i), \text{ where } \mathbf{D}_i = \mathbf{I}_i - \mathbf{I}_{i-1}, \quad i = 2, 3, \dots, t. \quad (4)$$

Tri-Modal Feature Fusion. Based on prior work [24, 25, 21], we first concatenate all the visual features of consecutive frames $\mathbf{F}_{1:t}^h$ and the motion features $\mathbf{F}_{2:t}^m$ along the channel dimension. To incorporate text semantic features, we insert the text embeddings $\mathbf{f}_{1:t}^{\text{text}}$ at the beginning of the token embedding sequence, yielding the final tri-modal fused features $\{\mathbf{f}_{1:t}^{\text{text}}, \mathbf{f}_{1:t}^{\text{cls}}, \mathbf{f}^1, \mathbf{f}^2, \dots, \mathbf{f}^{N_p}\}$. In the subsequent joint decoder, we simultaneously predict future vision and text modalities.

3.3 Sparse Feature Filtering Module

Bottleneck Feature Filter. Many previous works [10, 51, 25, 21, 52, 31, 28] utilize memory modules to memorize normal patterns, which often rely on well-predefined prototype quantities and struggle to handle complex and dynamic scenarios, otherwise, they may lead to excessive feature compression, or cause difficulties in training and excessive generalization ability.

Inspired by the bottleneck block [13, 15], we designed bottleneck feature filters. Without shortcuts, these filters learn to extract low-dimensional principal features through training on normal data to perform prediction tasks. Since they only learn the normal manifold, during the testing phase, anomalous information residing outside the representation space will be filtered out, causing anomalous events to be inaccurately predicted. We define the bottleneck feature filtering process BFF as follows:

$$\text{BFF}(\cdot) = \text{Expand}(\text{Act}(\text{Reduce}(\cdot))), \quad (5)$$

where $\text{Expand}(\cdot)$ and $\text{Reduce}(\cdot)$ denote the channel-wise expansion and reduction processes, respectively, and $\text{Act}(\cdot)$ represents the activation function.

Mixture of Feature Filtering Experts. In order to model the diversity and variation of normal patterns, an intuitive way is to horizontally stack multiple filters. However, directly expanding them horizontally is equivalent to increasing the width of the bottleneck, which would cause the bottleneck filtering operation to become ineffective. Inspired by the Mixture of Experts (MoE) architecture, we propose a sparse architecture that selectively routes through filtering modules via a gating mechanism while horizontally stacking filters, thereby implementing fine-grained feature filtering. Adopting an MoE architecture similar to [6], our proposed SFFM based on MoE can be formalized as follows:

$$\begin{cases} \mathbf{f}_{\text{out}} = \sum_{i=1}^{K_s} \text{BFF}_i(\mathbf{f}) + \sum_{i=K_s+1}^N (g_i \text{BFF}_i(\mathbf{f})), \\ g_i = \begin{cases} s_i, & s_i \in \text{Topk}(\{s_i \mid K_s + 1 \leq j \leq N\}, K - K_s), \\ 0, & \text{otherwise}, \end{cases} \\ s_i = \text{Softmax}_i(\text{Route}(\mathbf{f})), \end{cases} \quad (6)$$

where \mathbf{f} is the input feature, N denotes the total number of feature filtering experts, K_s represents the number of shared experts, BFF_i is the i -th bottleneck feature filter, g_i indicates the gating value for the i -th expert, s_i denotes the relevance score between the input feature and the i -th expert, the $\text{Topk}(\cdot, K)$ function computes the set of top- K highest relevance scores among all routing experts, and Route denotes the linear routing operation.

Following [6], we introduce the expert balance loss to alleviate the load imbalance problem:

$$\begin{cases} \mathcal{L}_{\text{ExpBal}} = \alpha \sum_{i=1}^N f_i p_i, \\ f_i = \frac{N - K_s}{(K - K_s)T} \sum_{t=1}^T \mathbb{1}(\text{Token } t \text{ selects Expert } i), \\ p_i = \frac{1}{T} \sum_{t=1}^T s_{i,t}, \end{cases} \quad (7)$$

where α is the expert balance factor, T is the total number of input tokens and $\mathbb{1}(\cdot)$ denotes the indicator function.

3.4 Multimodal Joint Decoding for Future Prediction

MJAD is a ViT architecture decoder Ψ similar to [12, 34], used to predict the next frame and semantic feature, ensuring mutual assistance among the appearance, motion, and semantic modalities, while

inserting an SFFM at each MJAD layer to perform feature filtering and compression. A patch expanding process is used to restore spatial size and output the predicted frame $\hat{\mathbf{I}}_{t+1}$, along with a feature projector to project semantic embeddings back to the original space, obtaining the predicted semantic features $\hat{\mathbf{f}}_{t+1}^{\text{text}}$. This process can be mathematically formalized as follows:

$$\hat{\mathbf{I}}_{t+1}, \hat{\mathbf{f}}_{t+1}^{\text{text}} = \Psi(\mathbf{f}_{1:t}^{\text{text}}, \mathbf{f}^{\text{cls}}, \mathbf{f}^1, \mathbf{f}^2, \dots, \mathbf{f}^{N_p}). \quad (8)$$

3.5 Inter-modality Consistency Constraint Mechanism

Basically, for the video prediction, we use the ℓ_2 distance between the predicted frame $\hat{\mathbf{I}}_{t+1}$ and the ground truth \mathbf{I}_{t+1} as the frame prediction loss:

$$\mathcal{L}_{\text{Pred}} = \left\| \mathbf{I}_{t+1} - \hat{\mathbf{I}}_{t+1} \right\|_2^2, \quad (9)$$

For the semantic modality, under normal circumstances, the previous continuous t -frame clip should be similar to the semantics of the next frame. The text semantic similarity is as follows:

$$\mathcal{L}_{\text{Sim}} = 1 - \frac{\mathbf{f}_{1:t}^{\text{text}} \cdot \hat{\mathbf{f}}_{t+1}^{\text{text}}}{\|\mathbf{f}_{1:t}^{\text{text}}\| \cdot \|\hat{\mathbf{f}}_{t+1}^{\text{text}}\|}, \quad (10)$$

Unlike previous works [24, 25] that directly reconstruct optical flow, we introduce a novel motion frame-difference contrastive loss: when the difference between the prediction $\hat{\mathbf{I}}_{t+1}$ and ground truth \mathbf{I}_{t+1} exceeds the difference between $\hat{\mathbf{I}}_{t+1}$ and the previous ground truth \mathbf{I}_t , we impose a penalty. This design offers two benefits: first, it indirectly enforces motion constraints in predictions. Second, it prevents the model from achieving low losses by merely mimicking the previous frame through skips, which are only used to restore appearance details. Otherwise, the decoder and filters would not work properly. The motion frame-difference contrastive loss is defined as:

$$\mathcal{L}_{\text{Motion}} = \max(0, (\hat{\mathbf{I}}_{t+1} - \mathbf{I}_{t+1})^2 - (\hat{\mathbf{I}}_{t+1} - \mathbf{I}_t)^2). \quad (11)$$

Comprehensively, the inter-modality consistency constraint mechanism is conducted as follows:

$$\mathcal{L} = \lambda_1 \mathcal{L}_{\text{Pred}} + \lambda_2 \mathcal{L}_{\text{Sim}} + \lambda_3 \mathcal{L}_{\text{Motion}} + \mathcal{L}_{\text{ExpBal}}, \quad (12)$$

where λ_1, λ_2 , and λ_3 are hyperparameters.

3.6 Anomaly Detection

During the testing phase, we measure anomaly scores based on prediction errors. We define the visual anomaly score \mathcal{S}_v and the semantic anomaly score \mathcal{S}_t as follows:

$$\mathcal{S}_v = \mathcal{G}(\left\| \mathbf{I}_{t+1} - \hat{\mathbf{I}}_{t+1} \right\|_2^2), \quad (13)$$

$$\mathcal{S}_t = \mathcal{G}(1 - \frac{\mathbf{f}_{1:t}^{\text{text}} \cdot \hat{\mathbf{f}}_{t+1}^{\text{text}}}{\|\mathbf{f}_{1:t}^{\text{text}}\| \cdot \|\hat{\mathbf{f}}_{t+1}^{\text{text}}\|}), \quad (14)$$

where $\mathcal{G}(\cdot)$ denotes the gaussian smoothing operation. We calculate the weighted sum as frame-level anomaly scores, with higher scores indicating more likely abnormalities: $\mathcal{S} = w_v \mathcal{S}_v + w_t \mathcal{S}_t$, where w_v and w_t are the weights of the two scores.

4 Experiments

4.1 Experimental Setup

Datasets. We validate the performance of the proposed method on the following three datasets:

- **ShanghaiTech** [24]: A highly challenging dataset containing 330 training videos and 130 test videos, spanning 13 distinct scenes and 130 types of abnormal events, such as chasing, fighting, cycling on sidewalks, etc.

Table 1: Comparison with SOTA methods on three datasets. **Bold** and underlined values represent the best and second-best performance, respectively.

Type	Method	Frame-Level AUC		
		ShanghaiTech	CUHK Avenue	UCSD Ped2
Object-centric	VEC[47]	74.8	90.2	97.3
	AED-SSMTL[9]	<u>82.4</u>	<u>91.5</u>	97.5
	HF ² -VAD[25]	76.2	91.1	99.3
	FBAE[2]	79.2	86.8	-
	MPT[36]	78.8	90.9	97.6
	SSAE[3]	80.5	90.2	-
Frame-centric	FFP[24]	72.8	84.9	95.4
	MemAE[10]	71.2	83.3	94.1
	MNAD[31]	72.8	88.5	97.0
	DLAN-AC[46]	74.7	89.9	97.6
	USTN-DSC[45]	73.8	89.9	98.1
	PDM-Net[16]	74.2	88.1	97.7
	AED-MAE[34]	79.1	91.3	95.4
	STNMamba[21]	74.9	89.0	98.0
	SFN-VAD (Ours)	83.0	91.6	<u>98.4</u>

- **CUHK Avenue** [26]: Includes 16 training videos and 21 test videos, all collected in campus scenarios. Anomaly types involve strange actions, throwing objects, etc.
- **UCSD Ped2** [19]: Contains 16 training videos and 12 test videos, captured in surveillance pedestrian walking areas. The dataset includes anomalies such as non-pedestrian objects (e.g., bicycles, cars) or abnormal pedestrian behaviors (e.g., running, skateboarding).

Evaluation Metric. We adopted the frame-level area under the curve (AUC) as the evaluation metric for the model. The AUC comprehensively evaluates model performance by calculating the area under the receiver operating characteristic (ROC) curve, which objectively reflects the model’s capability to distinguish between normal frames and anomalous frames.

Implementation Details. Our pretrained VLM utilizes InternVL2.5-1B [5]. SimCSE-BERT [8] is employed as the semantic encoder. In each SFFM, we default to 1 shared filtering expert and 63 routing filtering experts, with the top 7 routing experts activated based on the highest routing scores. Each feature filtering expert is a two-layer bottleneck MLP. The learning rate is set to 0.0002. $\lambda_1, \lambda_2, \lambda_3$ are all configured as 1, with an expert balance factor α of 0.001. For testing phases, the anomaly score weights (w_v, w_t) for Ped2, Avenue, and ShanghaiTech datasets are set to (0.8, 0.2), (0.9, 0.1), (0.2, 0.8), respectively. More details are in the appendix.

4.2 Comparison with State-of-the-art

We compare our method with SOTA methods on three benchmark datasets, including both object-centric [47, 9, 25, 2, 36, 3] and frame-centric methods [24, 10, 31, 46, 45, 16, 34, 21], covering representative memory-based methods [25, 10, 31, 46, 16, 21]. As shown in the table 1, our method consistently outperforms all frame-centric methods and most object-centric ones. Notably, on the challenging ShanghaiTech dataset, it achieves a SOTA frame-level AUC of 83.0, highlighting the effectiveness of our multimodal fusion and sparse feature filtering in complex scenarios. On Ped2, our method is slightly inferior to the object-centric optical flow method [25], which additionally introduces an optical flow estimator to capture the subtle direction and speed of pixel movement. Overall, our method achieves SOTA performance relying solely on frame-centric inputs, without the need to incorporate object detectors and independently compute anomaly scores for each one.

Table 2: Effectiveness analysis of multimodal branches on ShanghaiTech. Note that when the vision or semantic branches are removed, the corresponding decoding output is also removed.

Vision Branch	Semantic Branch	Motion Branch	AUC
✓			71.0
	✓		78.6
✓	✓		80.7
✓		✓	72.0
✓	✓	✓	83.0

Table 3: Ablation analysis of different parameter settings for the Mixture of Filtering Experts on ShanghaiTech. N_r , K , K_s respectively represent the total number of routing experts, activated routing experts and shared experts. Reduction Rate refers to the compression ratio of a single filter.

Strategy	K	N_r	K_s	Reduction Rate	AUC
w/o	0	0	0	-	79.5
Standard MLP	0	0	1	0.25	79.7
Bottleneck MLP	0	0	1	2	81.5
MoFE(2/16 + 0)	2	16	0	4	81.3
MoFE(1/15 + 1)	1	15	1	4	81.6
MoFE(3/31 + 1)	3	31	1	8	81.9
MoFE(7/63 + 1)	7	63	1	16	83.0

4.3 Ablation Study

Effectiveness of Multimodal Branches. We verified the effectiveness of three encoding branches on the most challenging ShanghaiTech dataset, as shown in Table 2. Firstly, when only the vision or motion branch is used, the performance remains relatively low, confirming the limitations of previous methods that focus solely on appearance and motion patterns. Introducing the semantic branch alone yields an AUC of 78.6, and after fusing with the vision branch, it reaches 80.7, verifying the representativeness advantage of semantic features for local abnormal events. When the three modalities work collaboratively, it jumps to 83.0, proving the effectiveness of full interaction and complementarity among multimodal features.

Impact of MoFE. Following [6], we validate the effectiveness of the Mixture of Filtering Experts and explore the impact of partitioning strategies. As shown in Table 3, “Standard MLP” indicates that the hidden dimension is four times that of the input and output dimensions, while “Bottleneck MLP” refers to a single feature filter. Experimental results show that the Bottleneck MLP significantly outperforms the standard MLP, thereby proving the effectiveness of our bottleneck filter. In addition, the best performance was achieved by gradually refining the expert partitioning, indicating that more detailed partitioning of each expert can achieve more professional and fine-grained feature filtering. Furthermore, when the shared expert is ignored, the performance slightly declines, which indicates that it is necessary to introduce shared filters to isolate multimodal shared knowledge.

Comparison with Memory Modules. To prove that our sparse feature filtering network outperforms the general memory modules, we imitate the previous method [25, 10, 31, 46, 16, 21] to set up a semantic memory and a vision memory at the bottleneck of our model for comparison. The results are shown in Table 4. Firstly, most of the memory methods are superior to the basic models without memory or SFFM, but the performance improvement is relatively small. Our SFFM is significantly superior to all memory methods, proving that the SFFM we proposed, can implement more diverse and specialized feature filtering mechanisms. Furthermore, we additionally replaced each SFFM in the decoder layer with the memory modules for a fairer comparison. Due to extreme information filtering, its performance is far lower than that of other methods.

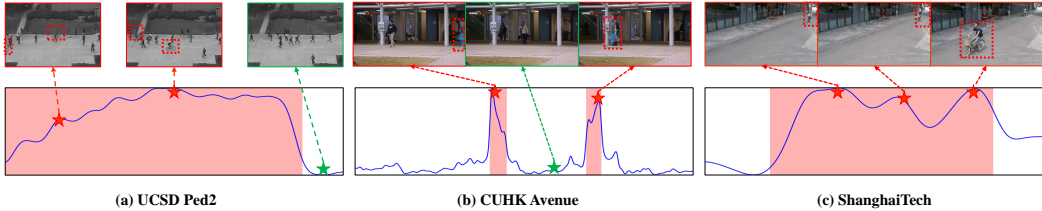


Figure 3: Visualization of anomaly score curves on UCSD Ped2 (a), CUHK Avenue (b), and ShanghaiTech (c). The red intervals indicate anomaly segments, the blue curve represents the computed anomaly scores, and the images above show the corresponding abnormal events (marked in red) or normal events (marked in green).

Table 4: Comparative analysis with memory modules on ShanghaiTech. “w/o” indicates not using the memory module or SFFM. “Multi-Level” means replacing each layer’s SFFM with a memory module.

Strategy	AUC
w/o	79.5
Memory(128 slots)	80.4
Memory(256 slots)	80.7
Memory(512 slots)	80.6
Memory(1024 slots)	80.0
Multi-Level Memory(256 slots)	70.4
SFFM	83.0

Table 5: Effectiveness analysis of loss function components on ShanghaiTech. Checkmarks (✓) indicate the use of corresponding losses, while their absence denotes exclusion. Notably, the prediction loss under the video prediction paradigm VAD must remain enabled.

$\mathcal{L}_{\text{Pred}}$	\mathcal{L}_{Sim}	$\mathcal{L}_{\text{Motion}}$	AUC
✓			72.2
✓		✓	72.3
✓	✓		81.5
✓	✓	✓	83.0

Effect of Loss Functions. We validate the effectiveness of our proposed text semantic similarity loss and motion frame difference loss in the VAD task. As shown in Table 5, when using only the frame prediction loss, the model’s AUC is 72.2, which increases to 72.3 when the motion loss is added. This indicates that merely relying on appearance and motion cannot effectively capture local anomalies in complex scenes. Upon incorporating the similarity loss with prediction loss, the performance significantly improves to 81.5, indicating the crucial role of semantics. When all three components are employed simultaneously, the AUC reaches 83.0, which proves that abnormal events can be better captured when the three modalities act together.

4.4 Visualization Analysis

Figure 3 visualizes the anomaly score curves obtained from the test videos. It can be seen that when anomalies occur, our method can detect them very well. Notably, even though the abnormal foreground objects are very small, the anomaly score generated by our method is still very high, which proves the effectiveness of SFN-VAD in capturing local abnormal behaviors in the entire frame. In Figure 4, we visualize the error maps between the predictions and the ground truth. It can be observed that the prediction errors are normally minimal. When anomalies occur, the predicted images show color changes, pixel shifts, and blurring, which appear as bright regions in the error maps. This validates that our method also excels in the spatial localization of abnormal events.

5 Conclusions

In this paper, we propose a semi-supervised VAD framework named SFN-VAD. By introducing a semantic branch that jointly utilizes appearance and motion to capture the high-level semantics in abnormal events, instead of relying solely on appearance and motion for insufficient local anomaly perception. Furthermore, we design a novel sparse feature filtering module to replace memory modules, achieving a more effective anomaly filtering mechanism. Extensive experiments demonstrate that our method surpasses existing state-of-the-art approaches. SFN-VAD pioneers the integration of semantic modalities into semi-supervised VAD and introduces a novel feature filtering paradigm

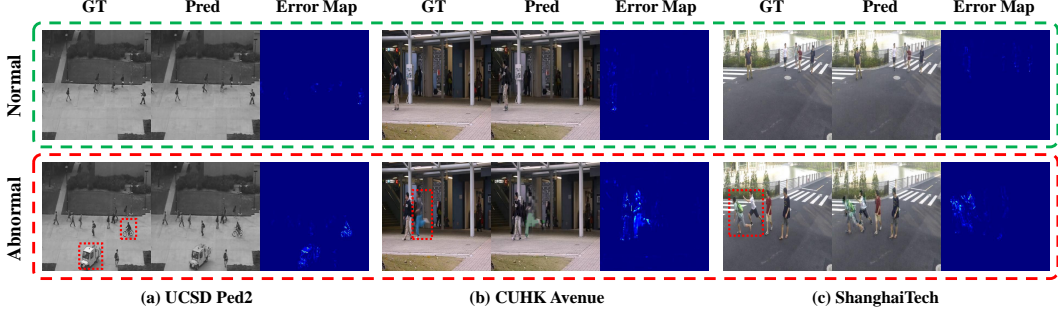


Figure 4: Visualization of predictions and error maps on UCSD Ped2 (a), CUHK Avenue (b), and ShanghaiTech (c). In the error maps, brighter areas indicate higher levels of abnormality in those regions.

based on the manifold space as an alternative to conventional memory modules. We believe this work will provide new perspectives for future research.

Acknowledgments and Disclosure of Funding

This work was supported by National Natural Science Foundation of China (NSFC) 62272172.

References

- [1] Shuai Bai, Keqin Chen, Xuejing Liu, Jialin Wang, Wenbin Ge, Sibo Song, Kai Dang, Peng Wang, Shijie Wang, Jun Tang, et al. Qwen2. 5-vl technical report. *arXiv preprint arXiv:2502.13923*, 2025.
- [2] Congqi Cao, Yue Lu, Peng Wang, and Yanning Zhang. A new comprehensive benchmark for semi-supervised video anomaly detection and anticipation. In *Proceedings of the IEEE/CVF conference on computer vision and pattern recognition*, pages 20392–20401, 2023.
- [3] Congqi Cao, Hanwen Zhang, Yue Lu, Peng Wang, and Yanning Zhang. Scene-dependent prediction in latent space for video anomaly detection and anticipation. *IEEE Transactions on Pattern Analysis and Machine Intelligence*, 2024.
- [4] Weiling Chen, Keng Teck Ma, Zi Jian Yew, Minhoe Hur, and David Khoo. Tevad: Improved video anomaly detection with captions. In *Proceedings of the IEEE/CVF Conference on Computer Vision and Pattern Recognition*, 2023.
- [5] Zhe Chen, Weiyun Wang, Yue Cao, Yangzhou Liu, Zhangwei Gao, Erfei Cui, Jinguo Zhu, Shenglong Ye, Hao Tian, Zhaoyang Liu, et al. Expanding performance boundaries of open-source multimodal models with model, data, and test-time scaling. *arXiv preprint arXiv:2412.05271*, 2024.
- [6] Damai Dai, Chengqi Deng, Chenggang Zhao, RX Xu, Huazuo Gao, Deli Chen, Jiashi Li, Wangding Zeng, Xingkai Yu, Yu Wu, et al. Deepseekmoe: Towards ultimate expert specialization in mixture-of-experts language models. *arXiv preprint arXiv:2401.06066*, 2024.
- [7] David Eigen, Marc'Aurelio Ranzato, and Ilya Sutskever. Learning factored representations in a deep mixture of experts. *arXiv preprint arXiv:1312.4314*, 2013.
- [8] Tianyu Gao, Xingcheng Yao, and Danqi Chen. Simcse: Simple contrastive learning of sentence embeddings. *arXiv preprint arXiv:2104.08821*, 2021.
- [9] Mariana-Iuliana Georgescu, Antonio Barbalau, Radu Tudor Ionescu, Fahad Shahbaz Khan, Marius Popescu, and Mubarak Shah. Anomaly detection in video via self-supervised and multi-task learning. In *Proceedings of the IEEE/CVF conference on computer vision and pattern recognition*, pages 12742–12752, 2021.
- [10] Dong Gong, Lingqiao Liu, Vuong Le, Budhaditya Saha, Moussa Reda Mansour, Svetha Venkatesh, and Anton van den Hengel. Memorizing normality to detect anomaly: Memory-augmented deep autoencoder for unsupervised anomaly detection. In *Proceedings of the IEEE/CVF international conference on computer vision*, pages 1705–1714, 2019.

[11] Mahmudul Hasan, Jonghyun Choi, Jan Neumann, Amit K Roy-Chowdhury, and Larry S Davis. Learning temporal regularity in video sequences. In *Proceedings of the IEEE conference on computer vision and pattern recognition*, pages 733–742, 2016.

[12] Kaiming He, Xinlei Chen, Saining Xie, Yanghao Li, Piotr Dollár, and Ross Girshick. Masked autoencoders are scalable vision learners. In *Proceedings of the IEEE/CVF conference on computer vision and pattern recognition*, pages 16000–16009, 2022.

[13] Kaiming He, Xiangyu Zhang, Shaoqing Ren, and Jian Sun. Deep residual learning for image recognition. In *Proceedings of the IEEE conference on computer vision and pattern recognition*, pages 770–778, 2016.

[14] Wenyi Hong, Weihan Wang, Ming Ding, Wenmeng Yu, Qingsong Lv, Yan Wang, Yean Cheng, Shiyu Huang, Junhui Ji, Zhao Xue, et al. Cogvlm2: Visual language models for image and video understanding. *arXiv preprint arXiv:2408.16500*, 2024.

[15] Andrew G Howard, Menglong Zhu, Bo Chen, Dmitry Kalenichenko, Weijun Wang, Tobias Weyand, Marco Andreetto, and Hartwig Adam. Movenets: Efficient convolutional neural networks for mobile vision applications. *arXiv preprint arXiv:1704.04861*, 2017.

[16] Chao Huang, Jie Wen, Chengliang Liu, and Yabo Liu. Long short-term dynamic prototype alignment learning for video anomaly detection. In *Proceedings of the Thirty-Third International Joint Conference on Artificial Intelligence*, pages 866–874, 2024.

[17] Michael I Jordan and Robert A Jacobs. Hierarchical mixtures of experts and the em algorithm. *Neural computation*, 6(2):181–214, 1994.

[18] Junnan Li, Dongxu Li, Silvio Savarese, and Steven Hoi. Blip-2: Bootstrapping language-image pre-training with frozen image encoders and large language models. In *International conference on machine learning*, pages 19730–19742. PMLR, 2023.

[19] Weixin Li, Vijay Mahadevan, and Nuno Vasconcelos. Anomaly detection and localization in crowded scenes. *IEEE transactions on pattern analysis and machine intelligence*, 36(1):18–32, 2013.

[20] Yunxin Li, Shenyuan Jiang, Baotian Hu, Longyue Wang, Wanqi Zhong, Wenhan Luo, Lin Ma, and Min Zhang. Uni-moe: Scaling unified multimodal llms with mixture of experts. *IEEE Transactions on Pattern Analysis and Machine Intelligence*, 2025.

[21] Zhangxun Li, Mengyang Zhao, Xuan Yang, Yang Liu, Jiamu Sheng, Xinhua Zeng, Tian Wang, Kewei Wu, and Yu-Gang Jiang. Stnmamba: Mamba-based spatial-temporal normality learning for video anomaly detection. *arXiv preprint arXiv:2412.20084*, 2024.

[22] Aixin Liu, Bei Feng, Bing Xue, Bingxuan Wang, Bochao Wu, Chengda Lu, Chenggang Zhao, Chengqi Deng, Chenyu Zhang, Chong Ruan, et al. Deepseek-v3 technical report. *arXiv preprint arXiv:2412.19437*, 2024.

[23] Haotian Liu, Chunyuan Li, Qingyang Wu, and Yong Jae Lee. Visual instruction tuning. *Advances in neural information processing systems*, 36:34892–34916, 2023.

[24] Wen Liu, Weixin Luo, Dongze Lian, and Shenghua Gao. Future frame prediction for anomaly detection—a new baseline. In *Proceedings of the IEEE conference on computer vision and pattern recognition*, pages 6536–6545, 2018.

[25] Zhian Liu, Yongwei Nie, Chengjiang Long, Qing Zhang, and Guiqing Li. A hybrid video anomaly detection framework via memory-augmented flow reconstruction and flow-guided frame prediction. In *Proceedings of the IEEE International Conference on Computer Vision*, 2021.

[26] Cewu Lu, Jianping Shi, and Jiaya Jia. Abnormal event detection at 150 fps in matlab. In *Proceedings of the IEEE international conference on computer vision*, pages 2720–2727, 2013.

[27] Haoyu Lu, Wen Liu, Bo Zhang, Bingxuan Wang, Kai Dong, Bo Liu, Jingxiang Sun, Tongzheng Ren, Zhuoshu Li, Hao Yang, et al. Deepseek-vl: towards real-world vision-language understanding. *arXiv preprint arXiv:2403.05525*, 2024.

[28] Hui Lv, Chen Chen, Zhen Cui, Chunyan Xu, Yong Li, and Jian Yang. Learning normal dynamics in videos with meta prototype network. In *Proceedings of the IEEE/CVF conference on computer vision and pattern recognition*, pages 15425–15434, 2021.

[29] Hui Lv and Qianru Sun. Video anomaly detection and explanation via large language models. *arXiv preprint arXiv:2401.05702*, 2024.

[30] Muhammad Maaz, Hanoona Rasheed, Salman Khan, and Fahad Shahbaz Khan. Video-chatgpt: Towards detailed video understanding via large vision and language models. *arXiv preprint arXiv:2306.05424*, 2023.

[31] Hyunjong Park, Jongyoun Noh, and Bumsub Ham. Learning memory-guided normality for anomaly detection. In *Proceedings of the IEEE/CVF conference on computer vision and pattern recognition*, pages 14372–14381, 2020.

[32] Yujiang Pu, Xiaoyu Wu, Lulu Yang, and Shengjin Wang. Learning prompt-enhanced context features for weakly-supervised video anomaly detection. *IEEE Transactions on Image Processing*, 2024.

[33] Alec Radford, Jong Wook Kim, Chris Hallacy, Aditya Ramesh, Gabriel Goh, Sandhini Agarwal, Girish Sastry, Amanda Askell, Pamela Mishkin, Jack Clark, et al. Learning transferable visual models from natural language supervision. In *International conference on machine learning*, pages 8748–8763. PMLR, 2021.

[34] Nicolae-C Ristea, Florinel-Alin Croitoru, Radu Tudor Ionescu, Marius Popescu, Fahad Shahbaz Khan, Mubarak Shah, et al. Self-distilled masked auto-encoders are efficient video anomaly detectors. In *Proceedings of the IEEE/CVF Conference on Computer Vision and Pattern Recognition*, pages 15984–15995, 2024.

[35] Leyang Shen, Gongwei Chen, Rui Shao, Weili Guan, and Liqiang Nie. Mome: Mixture of multimodal experts for generalist multimodal large language models. *arXiv preprint arXiv:2407.12709*, 2024.

[36] Chenrui Shi, Che Sun, Yuwei Wu, and Yunde Jia. Video anomaly detection via sequentially learning multiple pretext tasks. In *Proceedings of the IEEE/CVF International Conference on Computer Vision*, pages 10330–10340, 2023.

[37] Jiaqi Tang, Hao Lu, Ruizheng Wu, Xiaogang Xu, Ke Ma, Cheng Fang, Bin Guo, Jiangbo Lu, Qifeng Chen, and Yingcong Chen. Hawk: Learning to understand open-world video anomalies. *Advances in Neural Information Processing Systems*, 37:139751–139785, 2024.

[38] Wenhui Wang, Jifeng Dai, Zhe Chen, Zhenhang Huang, Zhiqi Li, Xizhou Zhu, Xiaowei Hu, Tong Lu, Lewei Lu, Hongsheng Li, et al. Internimage: Exploring large-scale vision foundation models with deformable convolutions. In *Proceedings of the IEEE/CVF conference on computer vision and pattern recognition*, pages 14408–14419, 2023.

[39] Yi Wang, Xinhao Li, Ziang Yan, Yinan He, Jiashuo Yu, Xiangyu Zeng, Chenting Wang, Changlian Ma, Haian Huang, Jianfei Gao, et al. Internvideo2. 5: Empowering video mllms with long and rich context modeling. *arXiv preprint arXiv:2501.12386*, 2025.

[40] Peng Wu, Chengyu Pan, Yuting Yan, Guansong Pang, Peng Wang, and Yanning Zhang. Deep learning for video anomaly detection: A review. *arXiv preprint arXiv:2409.05383*, 2024.

[41] Peng Wu, Xuerong Zhou, Guansong Pang, Zhiwei Yang, Qingsen Yan, Peng Wang, and Yanning Zhang. Weakly supervised video anomaly detection and localization with spatio-temporal prompts. In *Proceedings of the 32nd ACM International Conference on Multimedia*, pages 9301–9310, 2024.

[42] Peng Wu, Xuerong Zhou, Guansong Pang, Lingru Zhou, Qingsen Yan, Peng Wang, and Yanning Zhang. Vadclip: Adapting vision-language models for weakly supervised video anomaly detection. In *Proceedings of the AAAI Conference on Artificial Intelligence*, volume 38, pages 6074–6082, 2024.

[43] An Yang, Baosong Yang, Beichen Zhang, Binyuan Hui, Bo Zheng, Bowen Yu, Chengyuan Li, Dayiheng Liu, Fei Huang, Haoran Wei, et al. Qwen2. 5 technical report. *arXiv preprint arXiv:2412.15115*, 2024.

[44] Zhiwei Yang, Jing Liu, and Peng Wu. Text prompt with normality guidance for weakly supervised video anomaly detection. In *Proceedings of the IEEE/CVF Conference on Computer Vision and Pattern Recognition*, pages 18899–18908, 2024.

[45] Zhiwei Yang, Jing Liu, Zhaoyang Wu, Peng Wu, and Xiaotao Liu. Video event restoration based on keyframes for video anomaly detection. In *Proceedings of the IEEE/CVF Conference on Computer Vision and Pattern Recognition*, pages 14592–14601, 2023.

[46] Zhiwei Yang, Peng Wu, Jing Liu, and Xiaotao Liu. Dynamic local aggregation network with adaptive clusterer for anomaly detection. In *European Conference on Computer Vision*, pages 404–421. Springer, 2022.

- [47] Guang Yu, Siqi Wang, Zhiping Cai, En Zhu, Chuanfu Xu, Jianping Yin, and Marius Kloft. Cloze test helps: Effective video anomaly detection via learning to complete video events. In *Proceedings of the 28th ACM international conference on multimedia*, pages 583–591, 2020.
- [48] Tongtong Yuan, Xuange Zhang, Kun Liu, Bo Liu, Chen Chen, Jian Jin, and Zhenzhen Jiao. Towards surveillance video-and-language understanding: New dataset, baselines, and challenges, 2023.
- [49] Hang Zhang, Xin Li, and Lidong Bing. Video-llama: An instruction-tuned audio-visual language model for video understanding. *arXiv preprint arXiv:2306.02858*, 2023.
- [50] Huixin Zhang, Xiaohao Xu, Xiang Wang, Jialong Zuo, Chuchu Han, Xiaonan Huang, Changxin Gao, Yuehuan Wang, and Nong Sang. Holmes-vad: Towards unbiased and explainable video anomaly detection via multi-modal llm. *arXiv preprint arXiv:2406.12235*, 2024.
- [51] Mengyang Zhao, Yang Liu, Jing Liu, Di Li, and Xinhua Zeng. Lgn-net: Local-global normality network for video anomaly detection. *arXiv preprint arXiv:2211.07454*, 2022.
- [52] Hang Zhou, Jiale Cai, Yuteng Ye, Yonghui Feng, Chenxing Gao, Junqing Yu, Zikai Song, and Wei Yang. Video anomaly detection with motion and appearance guided patch diffusion model. In *Proceedings of the AAAI Conference on Artificial Intelligence*, volume 39, pages 10761–10769, 2025.

MemoryOut: Learning Principal Features via Multimodal Sparse Filtering Network for Semi-supervised Video Anomaly Detection (Appendix)

For a thorough understanding and visualization of our Multimodal Sparse Feature Filtering Network (SFN-VAD), we compile a comprehensive appendix. The following table of contents will direct you to specific sections of interest.

Contents

A Implementation Details	14
A.1 Tri-Modal Fusion Encoder	14
A.2 Sparse Feature Filtering Module	15
A.3 Multimodal Joint Attention Decoder	15
A.4 Experimental Details	16
B More Qualitative Results	17
B.1 Anomaly Localization	17
B.2 Anomaly Scoring	17
B.3 Ablation of Semantic Branch	18
B.4 Ablation of Motion Frame-difference Contrastive Loss	19
B.5 Compare with Memory Modules	19
B.6 Failure Case	20
C Limitations	21
D Broader Impact	21

A Implementation Details

A.1 Tri-Modal Fusion Encoder

The detailed architecture of the tri-modal fusion encoder is shown in Figure 5. For the vision appearance encoding branch, We directly apply the vision encoder from the VLM [5] to each input video frame. To match the VLM’s required input size, every frame is first resized to 448×448 pixels and then normalized. After passing through the encoder, each frame is mapped to a set of visual embeddings $\{h^{cls}, h^1, h^2, \dots, h^{N_p}\}$, where “cls” denotes the class token, N_p is the number of patches, and each token has dimensionality 1024.

For the text semantic encoding branch. The visual features produced above are projected and, together with a fixed prompt \mathbf{P} , fed into a language model [43] to generate a textual description of the video. To ensure steady outputs, we disable any sampling strategy and cap the generated text at a maximum length of 1024 tokens. The fixed prompt \mathbf{P} is: “*Describe the scene in the video segment, what objects are present, and what is each person doing?*”. We further employ a text encoder [8] to extract semantic features. This encoder uses contrastive learning to mitigate anisotropy in the semantic embeddings and to enhance the expressive power of the sentence representations. This step provides the foundational guarantee for all subsequent computations. Each descriptive text is encoded into a 768-dimensional semantic feature vector $\mathbf{f}_{1:t}^{text}$.

For the motion dynamic encoding branch, we use frame differences as input. Since each frame-difference map can likewise be treated as an image, we train a ViT-based encoder to extract motion information and align its spatial dimensions with those of the visual features. The motion encoder consists of four encoding layers. Each frame-difference map is encoded into motion embeddings $\{m^{cls}, m^1, m^2, \dots, m^{N_p}\}$, where “cls” denotes the class token and N_p represents the number of patches.

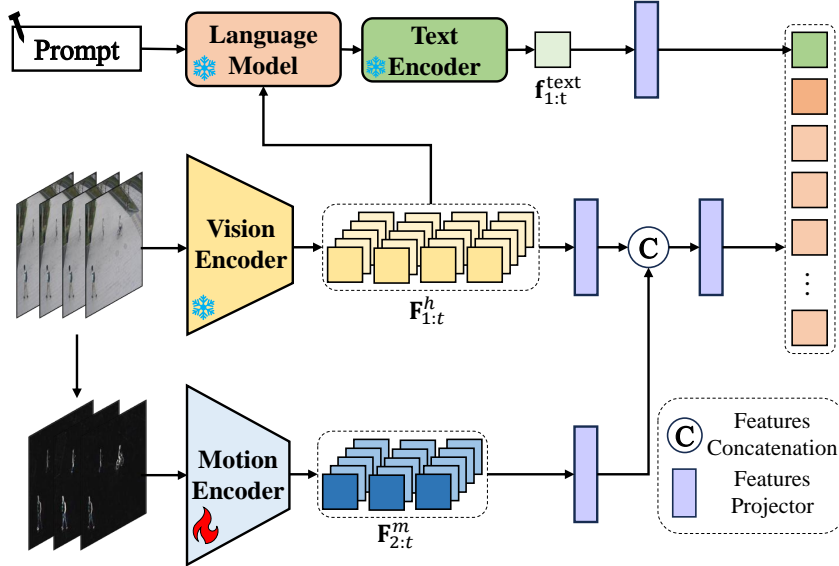


Figure 5: The architectural details of Tri-Modal Fusion Encoder.

We then fuse the outputs of the three branches to prepare for joint decoding. Concretely, we first project all modality features into the same dimensionality. Following previous practice, we concatenate the visual and motion features along the channel dimension and apply a projection layer to reproject the combined features into the same dimensions. This completes a simple temporal feature extraction and feature fusion process. Subsequently, the text semantic feature is inserted at the beginning of the token sequence, yielding the fused feature $\{f_{1:t}^{\text{text}}, f_{1:t}^{\text{cls}}, f^1, f^2, \dots, f^{N_p}\}$.

A.2 Sparse Feature Filtering Module

The detailed architecture of the Sparse Feature Filtering Module is shown in Figure 6. In this module, the bottleneck filter serves as its basic unit. Integrated into a mixture-of-experts framework, each bottleneck filter is assigned as a feature filtering expert responsible for the specialized extraction of the principal features. Concretely, each bottleneck filter is implemented as a bottleneck MLP consisting of two linear layers with a SiLU activation in between. The hidden-layer dimensionality is tuned per dataset to control the strength of feature filtering.

To further extend the capability of these bottleneck filters, we adopt a mixture-of-experts design akin to [6], subdividing experts more finely. By default, this architecture comprises 63 routing experts. For each input feature, a linear routing process computes its affinity to every expert; the top 7 experts (by gating score) are activated, and their outputs are combined via a softmax-weighted sum. Additionally, we include a shared filtering expert to capture common knowledge and boost the specialization of the routed experts during feature filtering.

A.3 Multimodal Joint Attention Decoder

The detailed architecture of the decoder is shown in Figure 7. Following [12, 34], we employ a ViT-based decoder to process the fused features. Its multi-head attention layers allow the fused features to interact with one another. Additionally, at each decoding layer, we insert a Sparse Feature Filtering Module to remove anomalous information. Because the model is trained exclusively on normal data, when anomalous behavior occurs the combined effects of multi-head attention and feature filtering will distort and disrupt the feature representations, thereby amplifying prediction errors and making abnormal versus normal events easier to distinguish.

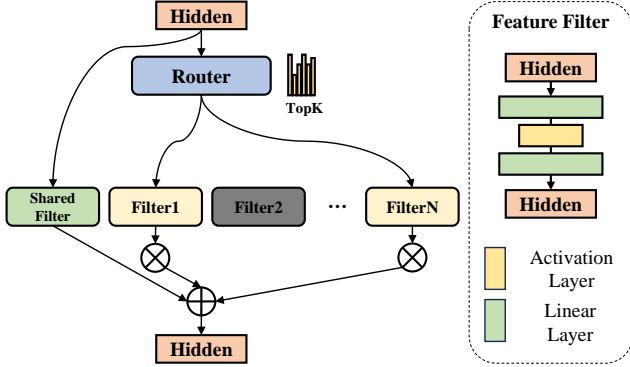


Figure 6: The architectural details of Sparse Feature Filtering Module.

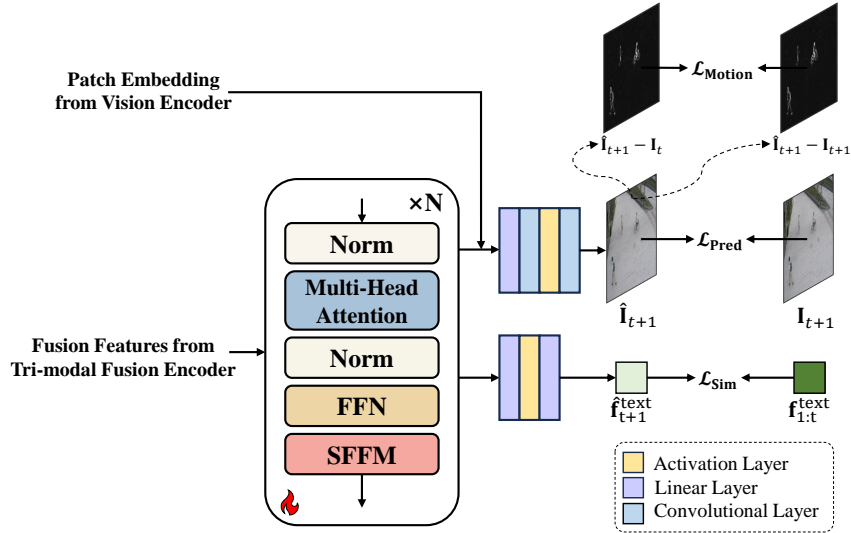


Figure 7: The architectural details of Multimodal Joint Attention Decoder.

A.4 Experimental Details

Our approach follows a prediction-based paradigm, utilizing $t = 4$ consecutive input frames to predict both the 5th frame and its semantic features. The frame error and semantic error jointly indicate anomaly confidence. We employ InternVL2.5-1B [5] as our pre-trained VLM and adopt SimCSE-BERT_{base} (trained on NLI datasets) [8] as the pre-trained text encoder.

For model optimization, we utilize the Adam optimizer with a base learning rate of 0.0002, momentum hyperparameters $\beta_1 = 0.9$ and $\beta_2 = 0.999$, coupled with L2 weight decay of 1×10^{-5} . The depth of the motion encoder and the multimodal joint attention decoder is set to four layers. Training epochs are configured as (1000, 10, 5) for UCSD Ped2, CUHK Avenue, and ShanghaiTech respectively. All frames are resized to 448×448 resolution with a batch size of 64. For the UCSD Ped2 and ShanghaiTech datasets, we set the reduction ratios of 32 and 16 for each bottleneck filtering expert according to the characteristics of each dataset. For CUHK Avenue, whose frame is comparatively narrow and where foreground objects occupy a relatively large portion of the view, an excessive reduction ratio would over-filter vital information; therefore, we use a reduction ratio of 4/3. The loss weighting factors λ_{Pred} , λ_{Sim} , λ_{Text} are all set to 1 with expert balance factor $\alpha = 0.001$. For testing phases, the anomaly score weights (w_v, w_t) for UCSD Ped2, CUHK Avenue, and ShanghaiTech datasets are set to $(0.8, 0.2)$, $(0.9, 0.1)$, $(0.2, 0.8)$, respectively. All experiments are conducted on dual Nvidia Geforce RTX 4090 GPUs.

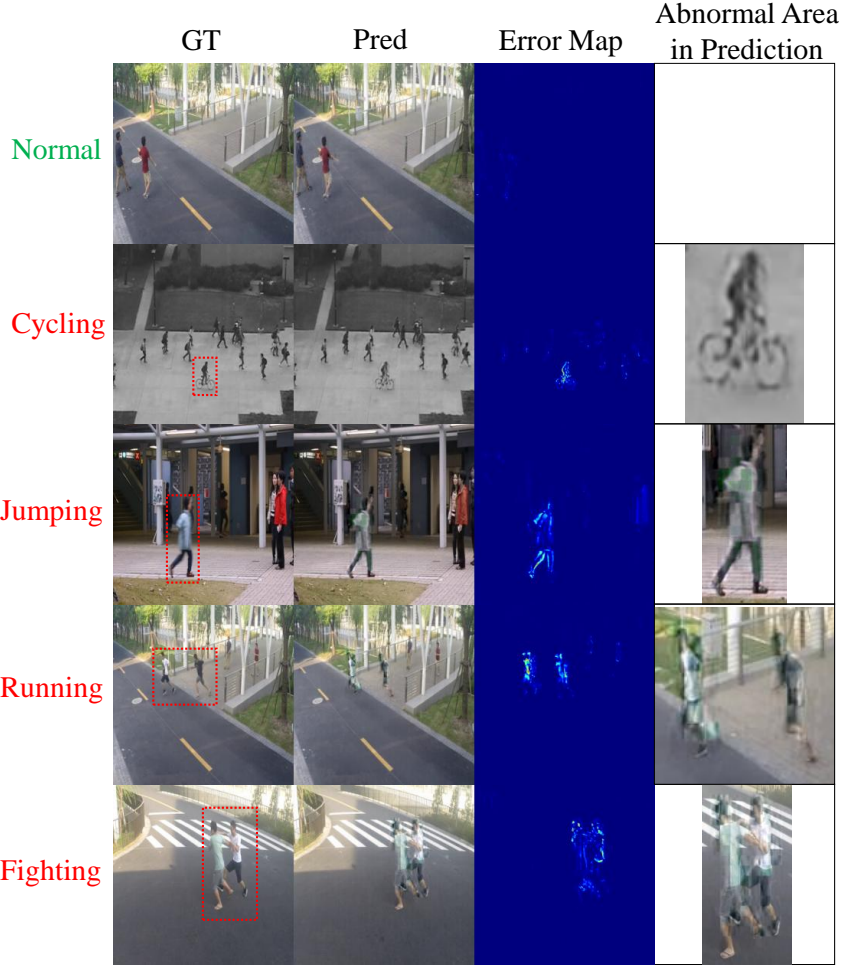


Figure 8: Examples of predictions and error maps for normal and different abnormal events.

B More Qualitative Results

B.1 Anomaly Localization

Figure 8 shows additional visualizations of our prediction results alongside their corresponding error maps relative to the ground truth. Under normal conditions (first row), the ground truth and predicted frames are virtually indistinguishable, and the error map is completely blue—indicating negligible error and no detected anomalies. Below, we present several examples of predicted abnormal events—cycling, jumping, running, and fighting. In the case of cycling, the anomaly manifests in two ways: bicycles never appear in the Ped2 training set, so their appearance deviates from the normal pattern, and their rapid motion differs from typical pedestrian movement on sidewalks; in the predicted frames, noticeable missing pixels and blurring around both the bicycle and rider confirm these deviations. Similarly, for jumping, running, and fighting, the regions of interest in the predicted frames exhibit clear distortions—shape warping, blurring, and misalignment—which are further highlighted in the error maps. These examples demonstrate that our method is also effective in spatially localizing abnormal events.

B.2 Anomaly Scoring

We present more anomaly score curves to further demonstrate the effectiveness of our method. In Figure 9, we show the anomaly score curve for test video **05_0018** from the ShanghaiTech dataset. In this video, an abnormal event occurs where pedestrians are seen chasing and playfully running

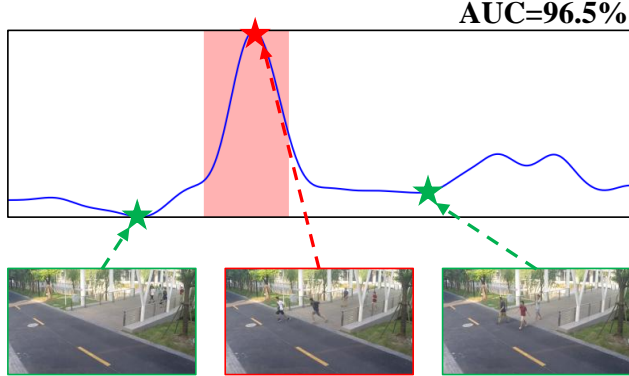


Figure 9: The anomaly score curve of the test video **05_0018** from ShanghaiTech. The red intervals indicate anomaly segments, the blue curve represents the computed anomaly scores, and the images above show the corresponding abnormal events (marked in red) or normal events (marked in green).

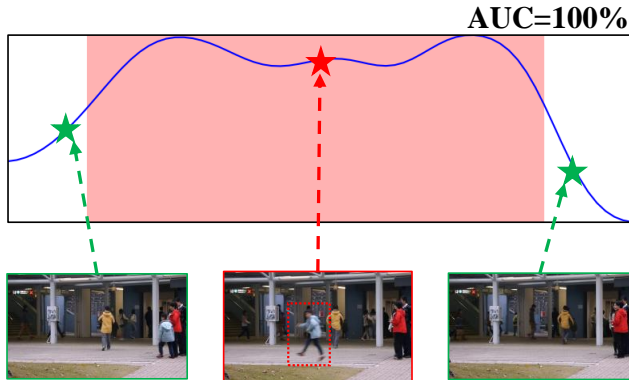


Figure 10: The anomaly score curve of the test video **21** from CUHK Avenue. The red intervals indicate anomaly segments, the blue curve represents the computed anomaly scores, and the images above show the corresponding abnormal events (marked in red) or normal events (marked in green).

on the road. Our method achieves an AUC score of 96.5% on this test sample, indicating that it can accurately distinguish between anomalous and normal frames, successfully identifying the people who are running and chasing.

In Figure 10, we present the anomaly score curve for test video **21** from the Avenue dataset. In this video, a child is seen jumping and playing on the sidewalk, which deviates from the normal pattern of pedestrians walking and is therefore considered abnormal behavior. As shown, our method achieves a perfect AUC score of 100% on this video, demonstrating its ability to accurately detect abnormal events.

In Figure 11, we show the anomaly score curve for test video **Test002** from the Ped2 dataset. In this video, an abnormal event is observed when a person is riding a bicycle in the pedestrian area. Our method is also able to perfectly identify and distinguish between normal and abnormal behaviors in this test sample, achieving an AUC of 100%.

B.3 Ablation of Semantic Branch

In Figure 12, we compare the anomaly score curves of our multimodal joint framework with the base model that includes only the appearance and semantic branches. The latter removes the semantic input and semantic prediction, using only frame prediction error as the anomaly score. As shown, in the early part of the video, a distant cyclist enters the sidewalk and is considered an anomaly. Our multimodal approach effectively detects this abnormal behavior and assigns it a high anomaly score. In contrast, the method without the semantic branch gives a much lower anomaly score. Later in the

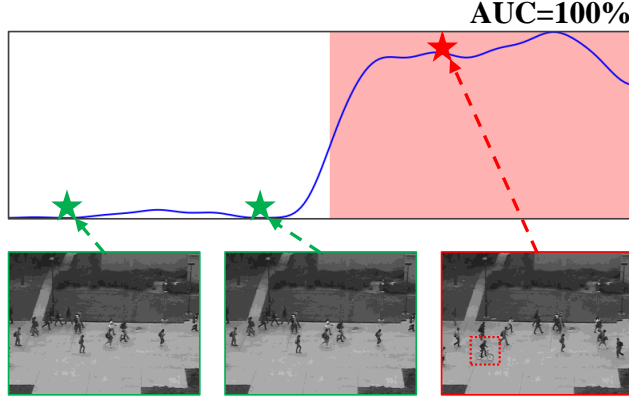


Figure 11: The anomaly score curve of the test video **Test002** from UCSD Ped2. The red intervals indicate anomaly segments, the blue curve represents the computed anomaly scores, and the images above show the corresponding abnormal events (marked in red) or normal events (marked in green)

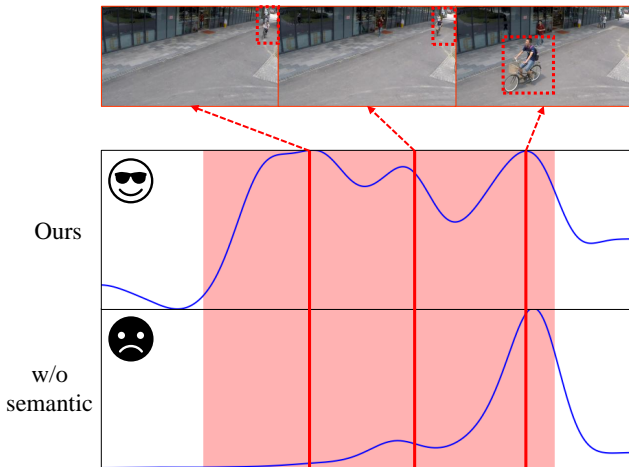


Figure 12: Ablation of Semantic Branch. The figure shows a comparison of anomaly score curves on the same test video between our multimodal framework and the method without the semantic branch.

video, another cyclist approaches the camera and occupies a larger portion of the frame. At this point, both methods are able to identify the anomaly more effectively. These observations demonstrate that existing methods struggle to detect localized anomalies with subtle motion, whereas our approach, by introducing a semantic branch, significantly enhances the ability to perceive such anomalies.

B.4 Ablation of Motion Frame-difference Contrastive Loss

As shown in Figure 13, we present the predicted frames with and without using the motion frame-difference contrastive loss. It can be observed that when abnormal behavior occurs, the predicted error for the abnormal object on the left is larger, with obvious pixel loss. In contrast, the prediction on the right retains more details around the edges of the abnormal object's body. This indicates that incorporating the motion frame-difference contrastive loss can effectively improve anomaly detection performance and suppress the model from simply relying on skip connections in the vision encoder to mimic the previous frame for prediction.

B.5 Compare with Memory Modules

As shown in Figure 14, a visual comparison between our method and the memory module-based method is presented. The blue curve represents the results computed by our method. Consistent with the experiments in the main paper, we removed all SFFMs and inserted memory modules of size 256



Figure 13: Ablation of Motion Frame-difference Contrastive Loss. The left side shows the prediction results with the motion frame-difference contrastive loss, while the right side shows the results without it. To enable a clearer comparison, one of the abnormal objects is enlarged.

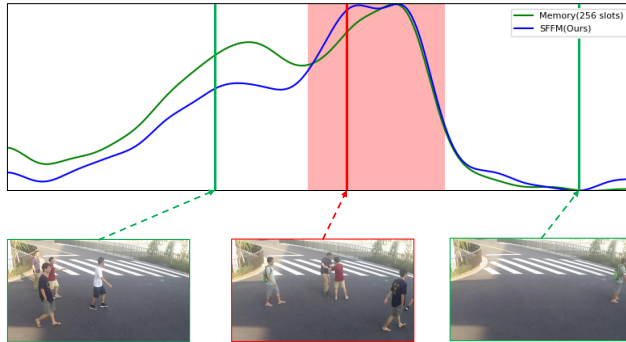


Figure 14: Comparative analysis with memory modules. The blue curve is obtained using our method, while the green curve is obtained by the memory-based method which removes the SFFM and inserts a memory module of size 256 between the encoder and decoder.

in both the encoder and decoder for comparison, resulting in the green curve. From the figure, it can be observed that in the early stages of the video, when no abnormal behavior has yet occurred, the anomaly scores calculated by our method are significantly lower than the memory-based method, reducing the possibility of false positives. Conversely, when abnormal events occur, the anomaly scores computed by our method are higher than those of the memory-based approach. This validates that the proposed SFFM achieves better anomaly detection performance than the memory module.

B.6 Failure Case

Although SFN-VAD is capable of accurately detecting most abnormal events, it occasionally fails to identify abnormal behaviors in some extreme scenarios. Figure 15 shows a failure case of our method on test video **12_0174** from the ShanghaiTech dataset. In this test video, the abnormal event involves a person riding a bicycle in a pedestrian area as shown, although our method is able to compute high anomaly scores at the early stage of the event, indicating that the abnormal behavior is initially well detected. However, the anomaly scores gradually decrease as the rider moves farther away and becomes smaller in the frame, eventually dropping to zero. This reveals a significant misjudgment issue, and the AUC metric for this video only reaches 81.9%.

This failure can be attributed to the fact that when the abnormal object is far away, it occupies a very small portion of the frame, which leads to two problems. First, the small size of the object results in very low frame prediction errors, as the static background dominates and averages out the prediction errors. Second, when the object is small, the VLM struggles to capture accurate semantic information about the abnormal object. It will also lead to a low semantic prediction error. Overall, even if we introduce semantics, it can to some extent solve the ability of appearance and motion to perceive local anomalies. However, when facing overly small foreground goals and the semantics cannot be well captured either, our multimodal framework will fail.

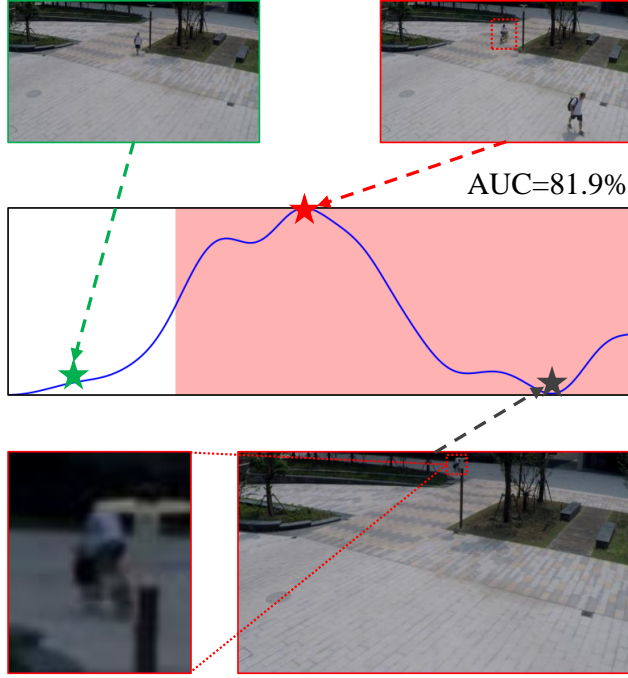


Figure 15: A failure case of our method.

We conjecture that further incorporating multi-scale temporal semantic information integration can help alleviate this issue. Specifically, in addition to the existing short-term window of 4 consecutive frames, temporal windows with larger time steps—such as 8 frames, 16 frames, 32 frames, and so on—can be constructed. Video descriptions can then be extracted from these different levels of frame sequences, and the semantic features from each level can be fused to capture the evolution of behavior over a longer temporal range within the scene. Furthermore, incorporating object-tracking techniques and integrating semantic information may further improve the accuracy of anomaly detection. However, the added complexity and computational overhead brought by the integration of multi-scale temporal semantics and object tracking pose significant challenges. Besides, how to effectively fuse semantic features from different levels remains a key challenge. We leave these considerations for future research.

C Limitations

The objective of this paper is frame-level video anomaly detection. By introducing a multimodal sparse filtering network, we have achieved enhanced performance in frame-level anomaly detection. Although spatial localization of anomalies within a frame can be accomplished using error maps, this method still has certain limitations when dealing with small objects. Furthermore, the detection of anomaly types holds significant importance for video anomaly detection systems. Future work needs to address the challenges of precise anomaly spatial localization and categorical differentiation of anomalous behaviors further.

D Broader Impact

SFN-VAD is a novel Video Anomaly Detection framework. By introducing semantic modalities and sparse feature filtering mechanisms, a high-performance frame-centric video anomaly detection capability has been achieved, bringing more diverse perspectives and contributions to the VAD field. This method is conducive to improving the system’s energy efficiency in scenarios such as monitoring security and network content review, efficiently detecting and identifying abnormal events in videos, and bringing beneficial social impacts.

However, like many video analysis technologies, SFN-VAD may raise concerns regarding privacy and potential misuse. In surveillance or content monitoring scenarios, the deployment of automated anomaly detection systems could lead to excessive data collection or surveillance overreach, especially without appropriate safeguards or oversight. We are committed to the ethical development and responsible deployment of our technology and will adhere to relevant data protection laws and industry best practices.